Hindawi
Journal of Nanomaterials
Volume 2022, Article ID 3147696, 21 pages
https://doi.org/10.1155/2022/3147696

Research Article

Triple Solutions with Stability Analysis of MHD Mixed Convection Flow of Micropolar Nanofluid with Radiation Effect

Hazoor Bux Lanjwani,[1] Muhammad Saleem Chandio,[1] M. Imran Anwar,[2] Amnah S. Al-Johani,[3] Ilyas Khan,[4] and Md. Nur Alam[5]

[1]*University of Sindh, Jamshoro, Pakistan*
[2]*University of Sargodha, Pakistan*
[3]*Mathematics Department, Faculty of Science, University of Tabuk, Tabuk, Saudi Arabia*
[4]*Department of Mathematics, College of Science Al-Zulfi, Majmaah University, Al-Majmaah 11952, Saudi Arabia*
[5]*Department of Mathematics, Pabna University of Science & Technology, Pabna-6600, Bangladesh*

Correspondence should be addressed to Ilyas Khan; i.said@mu.edu.sa and Md. Nur Alam; nuralam.pstu23@gmail.com

Received 16 October 2021; Revised 30 January 2022; Accepted 22 February 2022; Published 11 April 2022

Academic Editor: Raghvendra Bohara

This paper deals with two-dimensional steady boundary layer flow, heat, and mass transfer characteristics of micropolar nanofluid past on exponentially stretching/shrinking surface. The effect of different physical parameters like magnetic field, buoyancy, thermal radiation, and connective heat transfer are examined. Furthermore, similarity solutions are obtained by similarity transformation on the governing system of partial differential equations. The shooting method with help of the Maple software is used to achieve the numerical solutions of the equations. For the different ranges of the applied parameters, triple solutions are obtained for both cases of the surface. In view of the triple solutions, stability analysis is performed by bvp4c in the MATLAB software, where only first solution is found feasible which is discussed. The main findings of the first solution indicate the skin friction, drag force, heat, and mass transfer rates are increasing for the $\lambda > 0$ and decreasing for $\lambda < 0$ as the K is enhanced. The velocity profiles decrease with increase in magnetic, slip velocity, and suction parameters. The temperature profiles increase with increase in magnetic, thermophoresis, thermal radiation, and Brownian motion parameters, whereas concentration profiles reduce with increase in Schmitt number and Brownian motion.

1. Introduction

The study of non-Newtonian fluid flows have gained much importance, because of the common Newtonian fluids may not completely satisfy the properties of the fluid flow in many industrial applications, examples of such fluids are biological fluids, polymeric fluids, fluids containing additives, liquid crystals, and paint colloidal solutions. Moreover, the class of the non-Newtonian fluids containing different kinds of complex properties are Casson fluids, Maxwell fluids, and micropolar fluids. The micropolar fluid introduced by Eringen [1] possesses a microscopic effect due to the microstructure and micromotion of particles present in fluid. These microstructure particles are of different shapes which rotate independently to the motion of the fluid particles (Anwar et al. [2]). The system of the micropolar fluid flow equations contains a microrotating vector besides the classical velocity vector. These fluids contain smaller rigid particles which rotate about the centroid of volume particles that predicts the flow behaviors at rotation and microscale independently that is defined by a microrotation vector. Therefore, micropolar fluids are very important in fluid dynamics, especially in studying some flows around some important surfaces such as stretching surfaces or shrinking surfaces. In this regard, MHD micropolar fluid flow on the inclined plate was investigated by Kasim et al. [3]. The micropolar fluid flow on the inclined surface with different physical parameters was also studied by Das [4]. Srinivasacharya and Bindu [5] examined the entropic generation of the micropolar fluid with parallel plates on the inclined

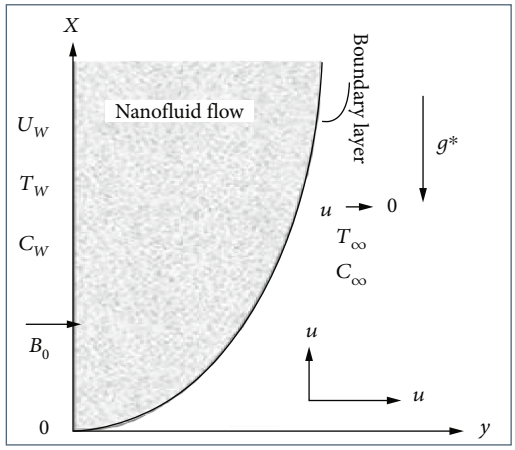

Figure 1: The flow model and the coordinate system.

Table 1: Comparison for the values of $-\theta(0)$ at different values of Pr, where N_t, R_d, and N_b are ignored.

Pr	$-\theta(0)$	
	Bidin and Nazar [20]	Present results
1	0.9547	0.9551
2	1.4714	1.4713
3	1.8691	1.8692

channel. Rahman et al. [6] examined the heat flux process in the micropolar fluid with incorporation different kinds of the fluid properties. Dero et al. [7] examined MHD micropolar nanofluid flow on exponential shrinking/stretching surface with radiation, Brownian motion, and thermophoresis effects. Srinivasacharya et al. [8] examined double diffusion impacts on the micropolar fluid flow on a slanted sheet. In [9], the authors studied peristaltic flow of nanofluids through a tapered channel with a porous medium.

Whereas magnetohydrodynamics (MHD) is concerned with physical and mathematical scaffold which shows magnetic dynamics in the electrical conducting fluid, the applications of magnetohydrodynamics are especially used in the modern industrial and engineering areas, such as in drawing of the plastic wires and films, polymer extrusion in melt spinning process, crystal growth, paper production and glass fiber, fluid film in the condensations processes, manufacturing in foods, electronic chips, electrochemical process, flow through the filtering devices, and thermal energy storage. Several investigators have worked on magnetohydrodynamics flow overstretching surfaces by using different physical parameters [10].

Moreover, nanotechnology has achieved much attention of the investigators because of having many applications in industrial and biological sciences. In industries, clay nanocomposites are used for the production of the impermeable wrapping films, silver nanoparticles are particularly used for productions of bins storage, while particles of the zinc oxides can be used for protection of the materials from the ultraviolet radiations and the carbon nanotubes pervaded graphite are used for the productions of light tennis rackets. In biological science, the investigators are busy developing the nanocapsules for the injections replacement that can be passed through the stomach and can accessed in the blood stream easily, whereas nanoparticles' antibacterial properties make them fit to cut and stitch the bandages. The nanofluid is a subclass of such a widely growing research field. Actually, nanofluids are engineered manufacturing fluids that are made by suspensions of the smallest sized particles (10^{-9} to 10^{-11} m) in common traditional fluids. Choi [11] called such flu as the fluids because of the addition of the smallest nanosized particles. Numerous engineering problems are studied by many researchers for more than two decades on the progress of nanofluids [12, 13], whereas the extensive convective rate of the heat transfers in nanofluids was studied by Buongiorno [14] by developing a two-phase nanofluid model. Furthermore, the boundary layer nanofluid flow phenomena on the shrinking/stretching surfaces have been discussed by many researchers [15, 16]. The nanofluid stagnation point flow was considered by Nazar et al. [17]. Kuznetsov and Nield [18] considered the boundary layer flow of the nanofluid through a vertically moving plate with buoyancy effect, while Chamkha et al. [19] considered mixed convective magnetohydrodynamics nanofluid flow with buoyancy effect by using Buongiorno's (2006) model.

Motivated from the abovementioned work, two-dimensional laminar magnetohydrodynamic boundary layer flow of micropolar nanofluid on exponentially shrinking/stretching surface with mixed convection, thermal radiation, magnetic, Brownian motion, and thermophoresis parameters has been studied. Furthermore, convective heat transfer and porous medium are also taken into account. There has been extension on the work done by Bidin and Nazar [20]. Their work was on the viscous fluid with unique solution while the present work is much updated. The graphical achieved results are used to study the influence of various physical parameters on the velocity, microrotation, temperature, and concentration profiles. Few other interesting studies in this direction are given in [21–24].

To the best of the authors' knowledge, such an attempt on MHD mixed convection flow of a micropolar nanofluid in the existence of the thermal radiation and magnetic field on an exponentially vertical stretching/shrinking surface by obtaining triple solutions with stability analysis has not been tried before. The results are demonstrated graphically with detailed discussion. It can be expected that the present research work will prove helpful for the researchers which are interested to study nanofluids particularly micropolar-based nanofluids as well as the importance of the stability analysis in case of the occurrence of multiple solutions, where stability analysis decides about real and extraneous solutions.

2. Problem Formulation

There is considered two-dimensional laminar magnetohydrodynamic (MHD) mixed convection flow, heat, and the mass transfer of the micropolar nanofluid on the permeable exponentially vertical shrinking/stretching surface with

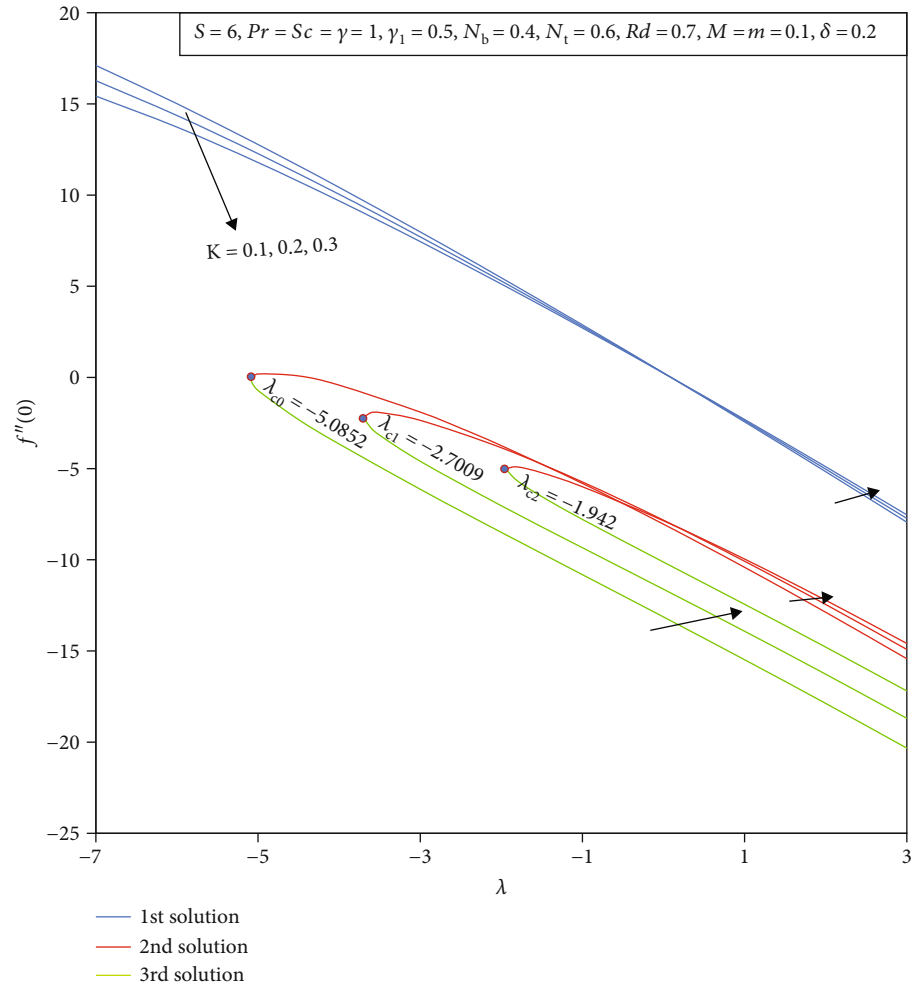

Figure 2: The effects of the K and λ on skin friction $(f''(0))$.

radiation effect. An electrically conducting nanofluid is considered with influence of the magnetic field $B(x)$ which is used perpendicular to the surface. The value of the Reynolds number is negligible that is ignored. The flow is considered along the x-axis perpendicular to the y-axis. The surface velocity is considered as $u_w(x) = U_w e^{x/L}$ at $y = 0$. A graphical presentation of flow model along the coordinate system is presented in Figure 1.

Applying boundary layer approximations, the continuity, momentum, microrotation, energy, and concentration equations for the micropolar nanofluid flow of present study are written as

$$\frac{\partial u}{\partial x} + \frac{\partial v}{\partial y} = 0, \tag{1}$$

$$u\frac{\partial u}{\partial x} + v\frac{\partial u}{\partial y} = \left(\vartheta + \frac{K_1}{\rho}\right)\frac{\partial^2 u}{\partial y^2} + \frac{K_1}{\rho}\frac{\partial N}{\partial y} - \frac{\sigma B_o^2(x)u}{\rho} + g^*\beta_T(T - T_\infty) + g^*\beta_c(C - C_\infty), \tag{2}$$

$$u\frac{\partial N}{\partial x} + v\frac{\partial N}{\partial y} = \frac{1}{\rho j}\left[\gamma^*\frac{\partial^2 N}{\partial y^2} - K_1\left(2N + \frac{\partial u}{\partial y}\right)\right], \tag{3}$$

$$u\frac{\partial T}{\partial x} + v\frac{\partial T}{\partial y} = \alpha\frac{\partial^2 T}{\partial y^2} + \tau_w\left[D_B\frac{\partial C}{\partial y}\frac{\partial T}{\partial y} + \frac{D_T}{T_\infty}\left(\frac{\partial T}{\partial y}\right)^2\right] - \frac{\vartheta}{c_p}\frac{\partial q_r}{\partial y}, \tag{4}$$

$$u\frac{\partial C}{\partial x} + v\frac{\partial C}{\partial y} = D_B\frac{\partial^2 C}{\partial y^2} + \frac{D_T}{T_\infty}\frac{\partial^2 T}{\partial y^2}, \tag{5}$$

where velocity components in the directions of the x and y are symbolized by u and v, respectively. σ is an electrical conduction, c_p is the specific heat of the constant pressure, ϑ is the kinematic viscosity, $B_o(x)$ is the constant of the magnetic field $B(x)$, β_T is the thermal expansion coefficient, β_C is concentration expansion coefficient, and ρ is the density of the fluid. N is the microrotation, K_1 is the vortex viscosity, γ^* represents the spin gradient viscosity, j is the ratio of microinertia, α is thermal diffusion, and k thermal conduction of the fluid. m is the constant whose range is $0 \le m \le 1$. Where at $m = 0$, there will be $N = 0$ that represents strong concentration that show no rotation due to microelements nearest to the solid surface, while $m = 1/2$ represents weaker concentration. Furthermore, $m = 1$ shows turbulences in flows of fluid (Ishak et al. [21]). Several researchers have taken $\gamma^* = (\mu + (K_1/2))j = \mu(1 + (K/2))j$, where $K_1 = \mu K$ is

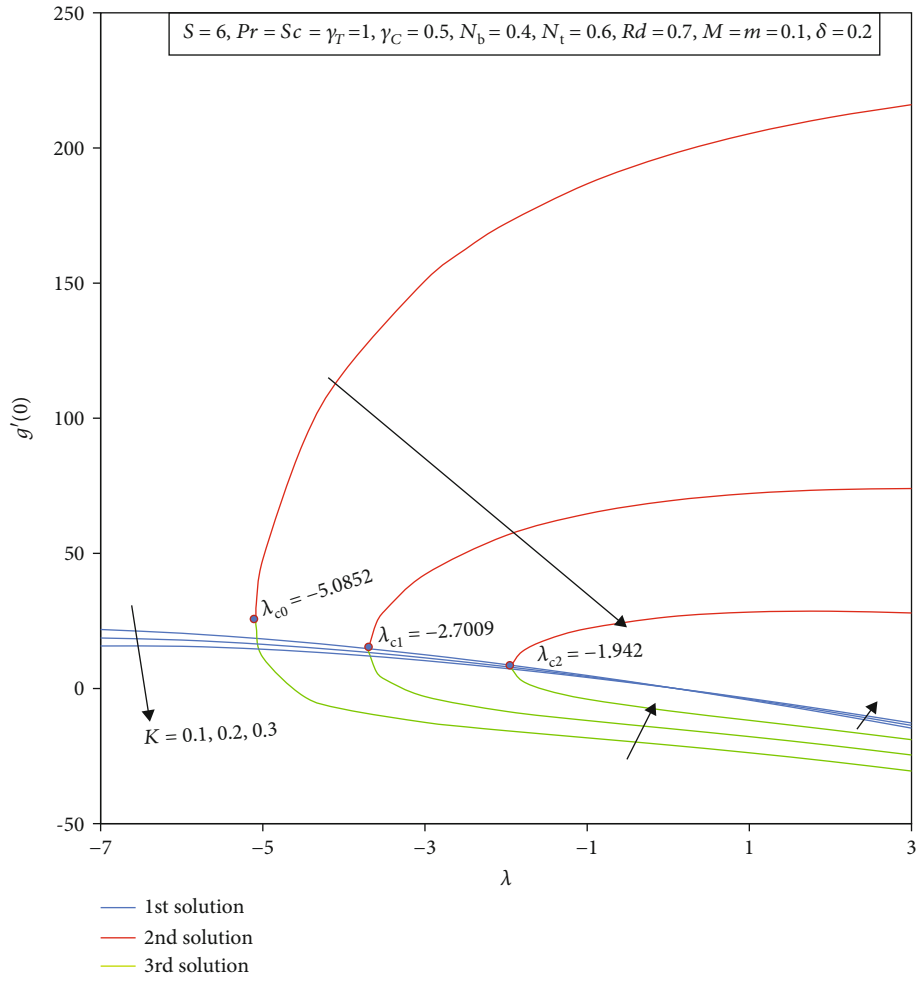

FIGURE 3: The effects of the K and λ on the couple stress $(g'(0))$.

the material parameter and $= 2lve^{-x/l}/U_w$. T is the temperature of the boundary layer flowing fluid, T_w is the surface temperature, T_∞ is the ambient fluid temperature, C is the nanoparticle volumetric fraction, q_r is the radiative thermal flux, and D_B and D_T are Brownian and thermophoresis diffusions coefficients, respectively. The radiative heat flux q_r is written by

$$q_r = \frac{4\sigma^*}{3k^*}\frac{\partial T^4}{\partial y}. \tag{6}$$

Here, k^* is a mean absorptions coefficient and σ^* is the Stefan Boltzmann constant. At smaller difference in the temperature of the flow, the T^4 will be described as the function of T. Using Taylor's series to T_∞ and by ignoring higher terms due to smallest values, we have

$$T^4 \cong 4T_\infty^3\, T - 3T^4. \tag{7}$$

By using Equations (5) and (6) in Equation (3), we get

$$\mathrm{u}\frac{\partial T}{\partial x} + v\frac{\partial T}{\partial y} = \alpha\left(1 + \frac{4.R_d}{3}\right)\frac{\partial^2 T}{\partial y^2} + \tau_w\left[D_B\left(\frac{\partial C}{\partial y}\frac{\partial T}{\partial y}\right) + \frac{D_T}{T_\infty}\left(\frac{\partial T}{\partial y}\right)^2\right]. \tag{8}$$

The considered boundary conditions of this problem are

$$v = v_w(x)\,; u = \lambda u_w(x) + A\frac{du}{dy},$$

$$N = -m\frac{\partial u}{\partial y},$$

$$T = T_w(x) = T_\infty + T_0\, e^{x/2l},$$

$$, C = C_w(x) = C_\infty + C_0 e^{x/2l} \text{at} y = 0,$$

$$u \longrightarrow 0\,; N \longrightarrow 0\,; T \longrightarrow T_\infty\,; C \longrightarrow C_\infty \text{ as } y \longrightarrow \infty. \tag{9}$$

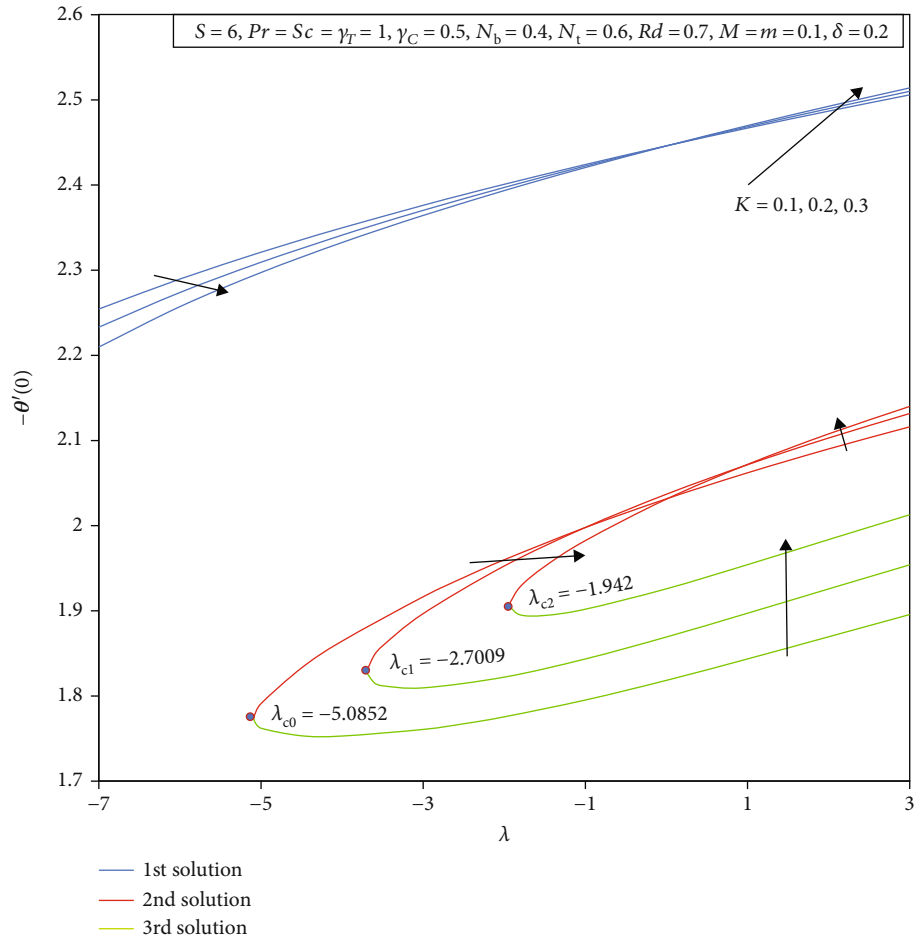

FIGURE 4: The effects of the K and λ on heat transfer rate $(-\theta'(0))$.

Magnetic field $B(x)$ for exponential surface is written as

$$B = B_0 e^{x/l}. \tag{10}$$

Furthermore, the following exponential type of the similarity transformation is applied to achieve the similarity solutions:

$$\psi = \sqrt{2\vartheta l U_w} e^{x/2L} f(\eta), \tag{11}$$

$$N = U_w e^{3x/2L} \sqrt{\frac{U_w}{2\vartheta L}} g(\eta), \tag{12}$$

$$\theta(\eta) = \frac{(T - T_\infty)}{(T_w - T_\infty)}, \tag{13}$$

$$\varnothing(\eta) = \frac{(C - C_\infty)}{(C_w - C_\infty)}, \tag{14}$$

$$\eta = y\sqrt{\frac{U_w}{2\vartheta L}} e^{x/2L}, \tag{15}$$

here, $\psi(x, y)$ is an stream function that in velocity form is defined as $u = \partial\psi/\partial y$ and $v = -\partial\psi/\partial x$. Thus, we get

$$\begin{aligned} u &= U_w e^{x/L} f'(\eta), \\ v &= -\sqrt{\frac{U_w \vartheta}{2L}} e^{x/2L} \left[f(\eta) + \eta f'(\eta) \right]. \end{aligned} \tag{16}$$

Whereas using Equation (15) in Equations (2) to (5), we get following system of equations:

$$(1 + K) f''' + f f'' - 2f'2 + Kg' - 2Mf' + 2\lambda_T \theta + 2\lambda_C \phi = 0, \tag{17}$$

$$\left(1 + \frac{K}{2}\right) g'' + f g' - 3g f' - 2Kg - Kf'' = 0, \tag{18}$$

$$\frac{1}{\mathrm{Pr}} \left(1 + \frac{4}{3} R_d\right) \theta'' + f\theta' + N_b \varnothing' \theta' + N_t \left(\theta'\right)^2 = 0, \tag{19}$$

$$\phi'' + \mathrm{Sc} f \phi' + \frac{N_t}{N_b} \theta'' = 0. \tag{20}$$

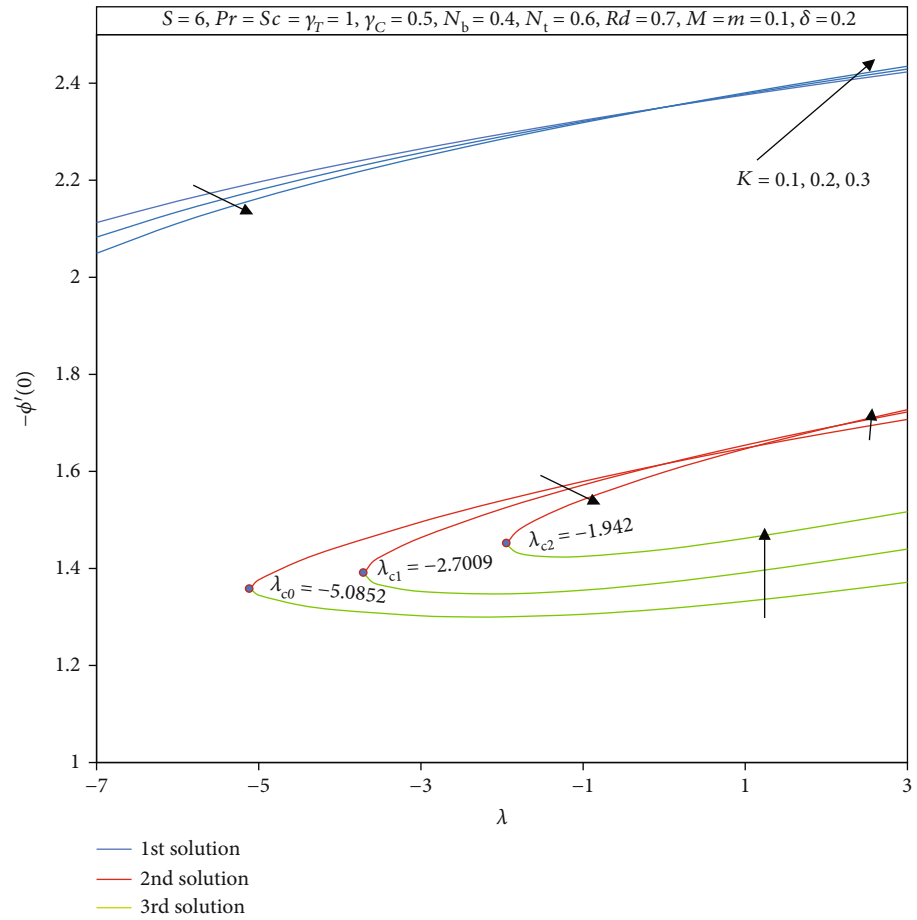

Figure 5: The effects of the K and λ on mass transfer rate $(-\phi'(0))$.

Boundary conditions take the form:

$$f(0) = S, f'(0) = \lambda + \delta f''(0), g(0) = -mf''(0), \theta'(0) = 1, \phi(0) = 1, \tag{21}$$

$$f'(\eta) \longrightarrow 0, g(\eta) \longrightarrow 0, \theta(\eta) \longrightarrow 0, \phi(\eta) \longrightarrow 0 \text{ as } \eta \longrightarrow \infty, \tag{22}$$

here, prime represents derivative along the η, $K = K_1/\mu$ is the non-Newtonian parameter, $\Pr = \vartheta/\alpha$ is the Prandtl number, $R_d = 4\sigma^* T_\infty^3/kk^*$ is the radiation parameter, $\mathrm{Sc} = \vartheta/D_B$ is the Schmidt number, $N_t = (\tau_w D_T(T_w - T_\infty))/\nu T_\infty$ is the thermophoresis parameter, $N_b = (\tau_w D_B(C_w - C_\infty))/\nu$ is the parameter of Brownian motion, λ is the shrinking/stretching surface, here $\lambda < 0$ denotes shrinking case and $\lambda > 0$ denotes stretching case and $S > 0$ denotes the suction of mass by the surface due to porosity, and $\delta = A\sqrt{U_w/\vartheta}$ is a velocity slip parameter. $\lambda_T = Gr/\mathrm{Re}_x^2 = (g^*\beta_T(T_w - T_\infty))/(u_w)^2$ where λ_T is ratio between buoyancy and inertia forces that is used as the criterion to create dominant regions of the forced and free convections. The $\lambda_T = 1$ stands for mixed (free and forced) convection and $\lambda_T = Gr/\mathrm{Re}_x^2 = (g^*\beta_T(T_w - T_\infty))/(u_w)^2$ stands for mass convective parameters. The skin friction coefficient (C_f), Nusselt number (Nu_x), and the Sherwood number (S_h) are written as

$$\begin{aligned} C_f &= \frac{[(\mu + K)(\partial u/\partial y) + KN]_{y=0}}{\rho u_w^2}, \\ \mathrm{Nu}_x &= \frac{-x(\partial T/\partial y)_{y=0}}{(T_w - T_\infty)}, \\ S_h &= \frac{-x(\partial C/\partial y)_{y=0}}{(C_w - C_\infty)}, \end{aligned} \tag{23}$$

using Equation (15), we get

$$\begin{aligned} C_f(\mathrm{Re}_x)^{1/2}\sqrt{\frac{2l}{x}} &= (1 + (1 - m)K)f''(0), \\ N_u(\mathrm{Re}_x)^{-1/2} &= -\theta'(0), \\ S_h(\mathrm{Re}_x)^{-1/2} &= -\varnothing'(0), \end{aligned} \tag{24}$$

where $\mathrm{Re}_x = u_w x/\vartheta$ is the Reynolds number.

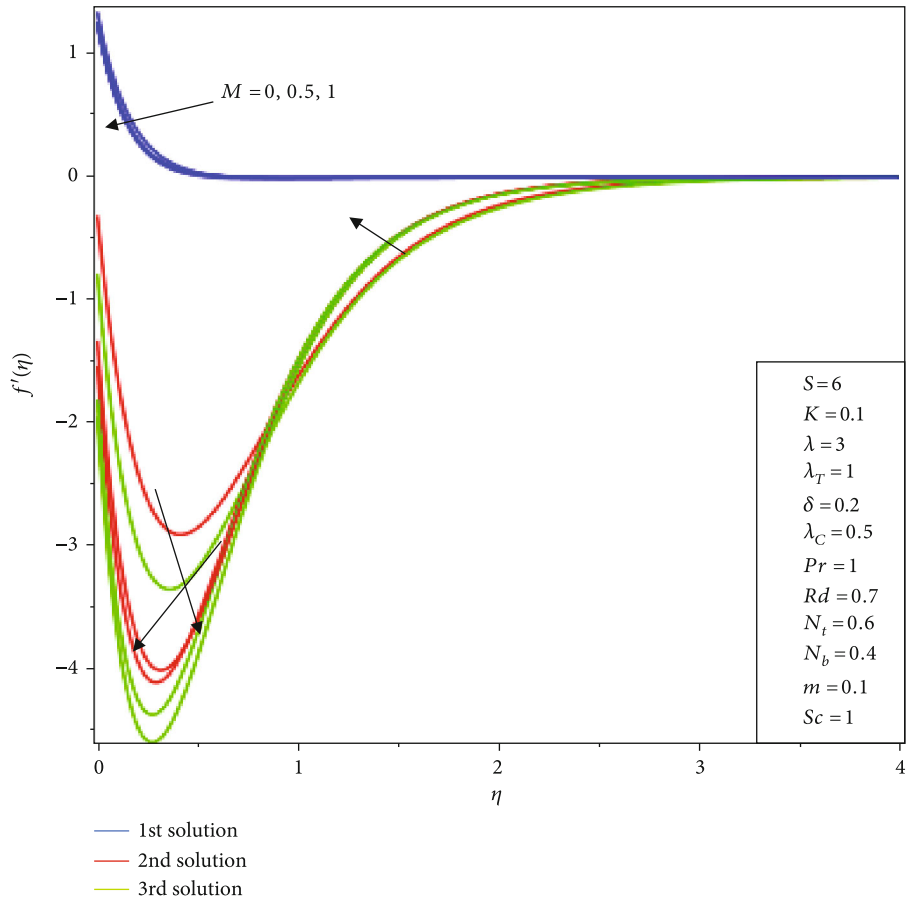

Figure 6: The effects of the M on velocity profiles $(f'(\eta))$.

3. Stability Analysis

To check the stability, there are taken unsteady case for Equations (2)–(5) with addition of the new time dependent variable τ as mentioned by Roşca and Pop [22].

$$\frac{\partial u}{\partial t} + u\frac{\partial u}{\partial x} + v\frac{\partial u}{\partial y} = \left(\vartheta + \frac{K_1}{\rho}\right)\frac{\partial^2 u}{\partial y^2} + \frac{K_1}{\rho}\frac{\partial N}{\partial y} - \frac{\sigma B^2 u}{\rho} + g^*\beta_C(T - T_\infty) + g^*\beta_C(C - C_\infty), \tag{25}$$

$$\frac{\partial N}{\partial t} + u\frac{\partial N}{\partial x} + v\frac{\partial N}{\partial y} = \frac{1}{\rho j}\left[\gamma^*\frac{\partial^2 N}{\partial y^2} - \kappa\left(2N + \frac{\partial u}{\partial y}\right)\right], \tag{26}$$

$$\frac{\partial T}{\partial t} + u\frac{\partial T}{\partial x} + v\frac{\partial T}{\partial y} = \left(\alpha + \frac{16\sigma^* T_\infty^3}{3K^*\rho c_p}\right)\frac{\partial^2 T}{\partial y^2} + \tau_w\left[D_B\frac{\partial C}{\partial y}\frac{\partial T}{\partial y} + \frac{D_T}{T_\infty}\left(\frac{\partial T}{\partial y}\right)^2\right], \tag{27}$$

$$\frac{\partial C}{\partial t} + u\frac{\partial C}{\partial x} + v\frac{\partial C}{\partial y} = D_B\frac{\partial^2 C}{\partial y^2} + \frac{D_T}{T_\infty}\frac{\partial^2 T}{\partial y^2}. \tag{28}$$

To get the similarity equations, the similarity transformation (15) takes the form as follows:

$$\psi = \sqrt{2\vartheta l U_w}\, e^{x/2l} f(\eta, \tau)\,; N = U_w e^{3x/2l}\sqrt{\frac{U_w}{2\vartheta l}}\, g(\eta, \tau), \tag{29}$$

$$\theta(\eta, \tau) = \frac{(T - T_\infty)}{(T_w - T_\infty)}, \tag{30}$$

$$\varnothing(\eta, \tau) = \frac{(C - C_\infty)}{(C_w - C_\infty)}, \tag{31}$$

$$\eta = y\sqrt{\frac{U_w}{2\vartheta l}}e^{x/2l}, \tag{32}$$

$$\tau = \frac{U_w}{2l}e^{x/l}.t. \tag{33}$$

Using Equation (33) in Equations (25)–(28), the following is obtained:

$$(1 + K)\frac{\partial^3 f}{\partial \eta^3} - 2\left(\frac{\partial f}{\partial \eta}\right)^2 - 2\tau\frac{\partial f}{\partial \eta}\frac{\partial^2 f}{\partial \eta \partial \tau} + f\frac{\partial^2 f}{\partial \eta^2} + K\frac{\partial g}{\partial \eta} - M\frac{\partial f}{\partial \eta} + 2\lambda_T\theta(\eta) + 2\lambda_C\varnothing(\eta) - \frac{\partial^2 f}{\partial \eta \partial \tau} = 0, \tag{34}$$

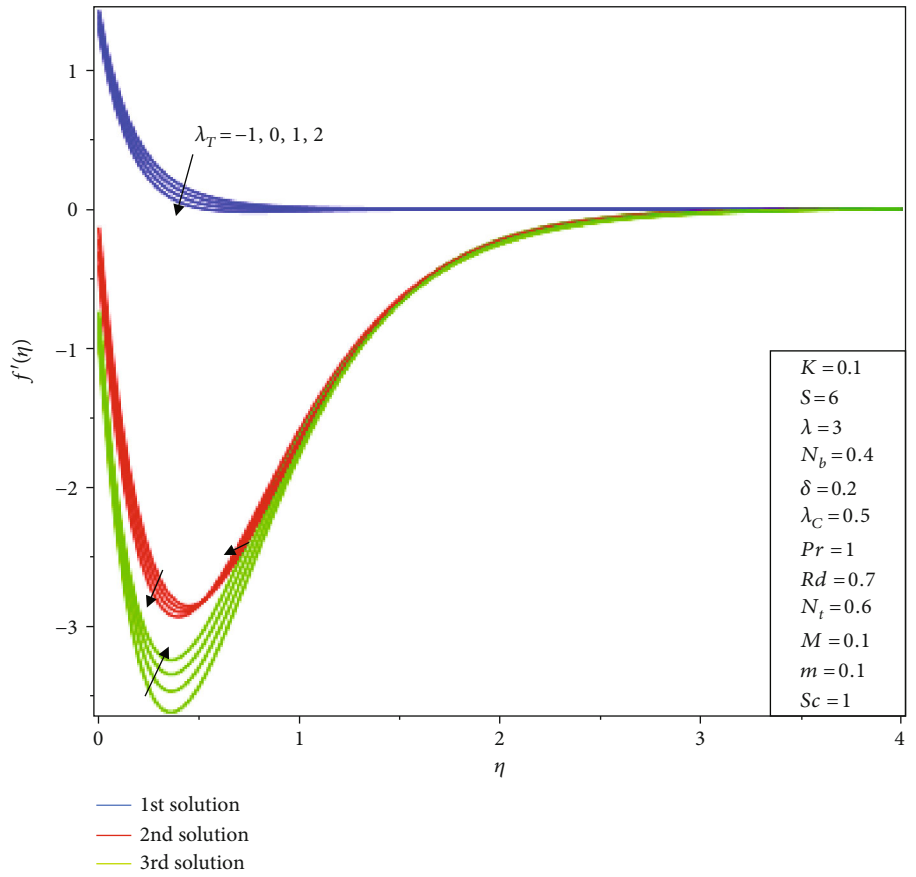

Figure 7: The effects of the λ_T on the velocity profiles $(f'(\eta))$.

$$\left(1+\frac{K}{2}\right)\frac{\partial^2 g}{\partial \eta^2} + f\frac{\partial g}{\partial \eta} - 3\frac{\partial f}{\partial \eta}.g - 2\tau\frac{\partial f}{\partial \eta}.\frac{\partial g}{\partial \tau} - 2Kg - K\frac{\partial^2 f}{\partial \eta^2} - \frac{\partial g}{\partial \tau} = 0, \tag{35}$$

$$\frac{1}{\Pr}\left(1+\frac{4R_d}{3}\right)\frac{\partial^2 \theta}{\partial \eta^2} - 2\tau\frac{\partial f}{\partial \eta}\frac{\partial \theta}{\partial \tau} + f\frac{\partial \theta}{\partial \eta} + N_b\frac{\partial \varnothing}{\partial \eta}\frac{\partial \theta}{\partial \eta} + N_t\left(\frac{\partial \theta}{\partial \eta}\right)^2 - \frac{\partial \theta}{\partial \tau} = 0, \tag{36}$$

$$\frac{\partial^2 \varnothing}{\partial \eta^2} + \mathrm{Sc}f\frac{\partial \varnothing}{\partial \eta} - 2\tau\mathrm{Sc}\frac{\partial f}{\partial \eta}\frac{\partial \varnothing}{\partial \tau} + \frac{N_t}{N_b}\frac{\partial^2 \theta}{\partial \eta^2} - \frac{\partial \varnothing}{\partial \tau} = 0. \tag{37}$$

The boundary conditions given in Equation (21) are written as

$$\mathrm{f}(0,\tau) = S, \tag{38}$$

$$\frac{\partial f(0,\tau)}{\partial \eta} = \lambda + \delta\frac{\partial^2 f(0,\tau)}{\partial \eta^2}, \tag{39}$$

$$g(0,\tau) = -m\frac{\partial^2 f(0,\tau)}{\partial \eta^2}, \tag{40}$$

$$\frac{\partial \theta(0,\tau)}{\partial \eta} = 1, \varnothing(0,\tau) = 1, \tag{41}$$

$$\frac{\partial f(\eta,\tau)}{\partial \eta} \longrightarrow 0, g(\eta,\tau) \longrightarrow 0, \theta(\eta,\tau) \longrightarrow 0, \varnothing(0,\tau) \longrightarrow 0 \text{ as } \eta \longrightarrow \infty. \tag{42}$$

For the stability of steady flow solutions $f(\eta) = f_0(\eta)$, $g(\eta) = g_0(\eta)$, $\theta(\eta) = \theta_0(\eta)$, and $\varnothing(\eta) = \varnothing_0(\eta)$ which placate the problem given in Equations (17)–(21), we further define

$$\begin{aligned} f(\eta,\tau) - e^{-\gamma\tau}F(\eta,\tau) &= f_0(\eta), \\ g(\eta,\tau) - e^{-\gamma\tau}G(\eta,\tau) &= g_0(\eta), \\ \theta(\eta,\tau) - e^{-\gamma\tau}H(\eta,\tau) &= \theta_0(\eta), \\ \varnothing(\eta,\tau) - e^{-\gamma\tau}S(\eta,\tau) &= \varnothing_0(\eta), \end{aligned} \tag{43}$$

where γ denotes unknown eigenvalues and $F(\eta,\tau)$, $G(\eta,\tau)$, $H(\eta,\tau)$, and $S(\eta,\tau)$ are smaller functions related to the $f_0(\eta)$, $g_0(\eta)$, $\theta_0(\eta)$, and $\varnothing_0(\eta)$, respectively. By substitution of Equation (43) in Equations (34)–(42), we have

$$\begin{aligned} &(1+K)F_0''' + f_0F_0'' + f_0''F_0 - 4f_0'F_0' + KG_0' - MF_0' + 2\lambda_T H_0 + 2\lambda_C S_0 + 2\gamma\tau f_0'G_0 + \gamma F_0' = 0, \\ &\left(1+\frac{K}{2}\right)G_0'' + f_0G_0' + F_0g_0' - 3f_0'G_0 - 3g_0F_0' - 2KG_0 - KF_0'' + 2\gamma\tau f_0'G_0 + \gamma G_0 = 0, \\ &\frac{1}{\Pr}\left(1+\frac{4}{3}R_d\right)H_0'' + f_0H_0' + F_0\theta_0' + N_b\varnothing_0'H_0' + N_bS_0'\theta_0' + N_t\theta_0'H_0' + 2\gamma\tau f'_0H_0 + \gamma H_0 = 0, \\ &S_0'' + Sc\left\{\left(f_0S_0' + F_0\varnothing_0'\right)\right\} + \frac{N_t}{N_b}H_0'' + 2Sc\gamma\tau f'_0S_0 + \gamma S_0 = 0. \end{aligned} \tag{44}$$

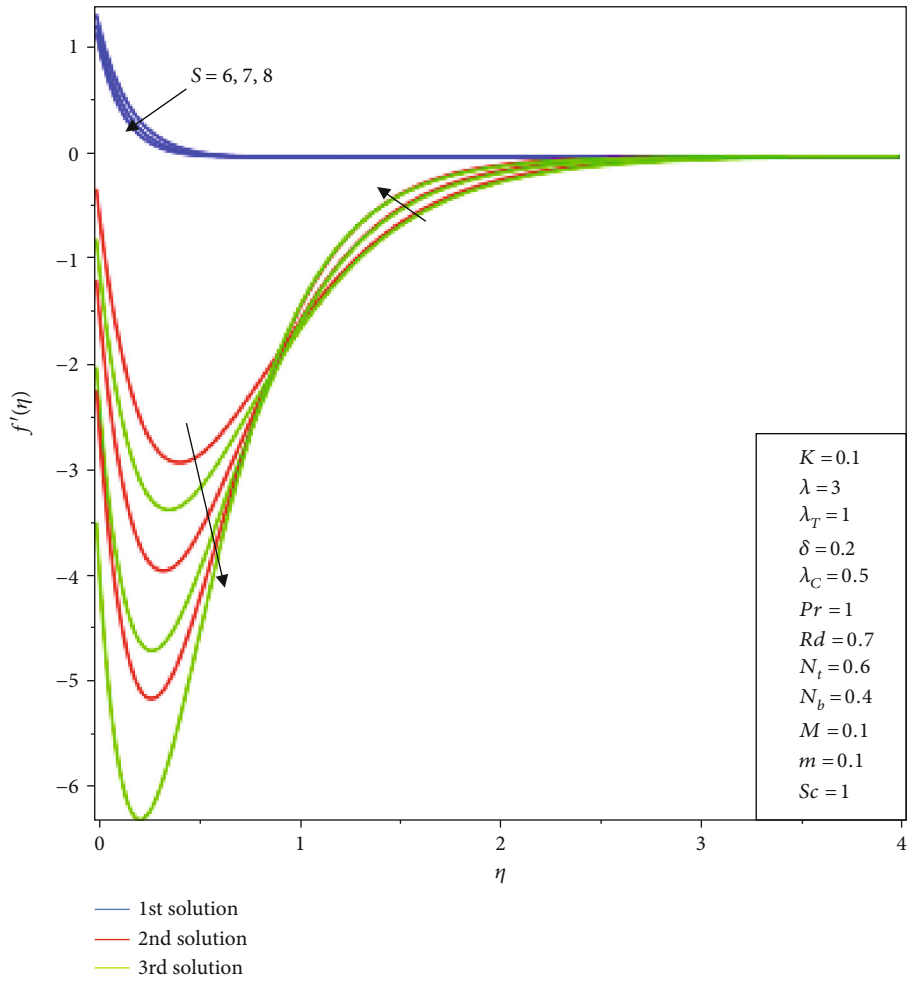

Figure 8: The effects of the S on the velocity profiles $(f'(\eta))$.

For to be achieved steady solution, there will be taken $\tau = 0$, so, we get

$$(1+K)F_0''' + f_0F_0'' + f_0''F_0 - 4f_0'F_0' + KG_0' - MF_0' + 2\lambda_T H_0 + 2\lambda_C S_0 + \gamma F_0' = 0, \tag{45}$$

$$\left(1+\frac{K}{2}\right)G_0'' + f_0G_0' + F_0g_0' - 3f_0'G_0 - 3g_0F_0' - 2KG_0 - KF_0'' + \gamma G_0 = 0, \tag{46}$$

$$\frac{1}{\Pr}\left(1+\frac{4}{3}R_d\right)H_0'' + f_0H_0' + F_0\theta_0' + N_b\varnothing_0'H_0' + N_bS_0'\theta_0' + N_t\theta_0'H_0' + \gamma H_0 = 0, \tag{47}$$

$$S_0'' + Sc\left\{\left(f_0S_0' + F_0\varnothing_0'\right)\right\} + \frac{N_t}{N_b}H_0'' + \gamma S_0 = 0, \tag{48}$$

Boundary conditions are

$$F_0(0) = 0\,;\, F_0'(0) = \delta F_0''(0)\,;\, F_0'(\eta) \longrightarrow 0 \text{ as } \eta \longrightarrow \infty, \tag{49}$$

$$G_0(0) = -mF_0''(0)\,;\, G_0(\eta) \longrightarrow 0 \text{ as } \eta \longrightarrow \infty, \tag{50}$$

$$H_0(0) = 0\,;\, H_0(\eta) \longrightarrow 0 \text{ as } \eta \longrightarrow \infty, \tag{51}$$

$$S_0(0) = 0\,;\, S_0(\eta) \longrightarrow 0 \text{ as } \eta \longrightarrow \infty. \tag{52}$$

Solutions of the eigenvalue problem of Equations (45)–(48) that satisfy Equations (49) are achieved by the solver functions of bvp4c through MATLAB software. These solutions provide a set of eigenvalues $\gamma_1 < \gamma_2 < \gamma_3$. According to Harris et al. [23], the required smallest eigenvalue can be obtained by relaxing one of boundary condition to initial condition. In this regard, in the present problem, we have relaxed $F_0'(\eta) \longrightarrow 0$ as $\eta \longrightarrow \infty$ in the form of the $F_0''(0) = 1$. Where the smallest positive values of the γ_1 demonstrates initial deterioration of the disturbance, the solutions concerned to the flow possessing smallest positive eigenvalues are considered physically feasible and stable. Converse to it, the negative γ_1 demonstrates initial growth of the disorder; therefore, solutions of the fluid flow are considered not practically feasible and unstable.

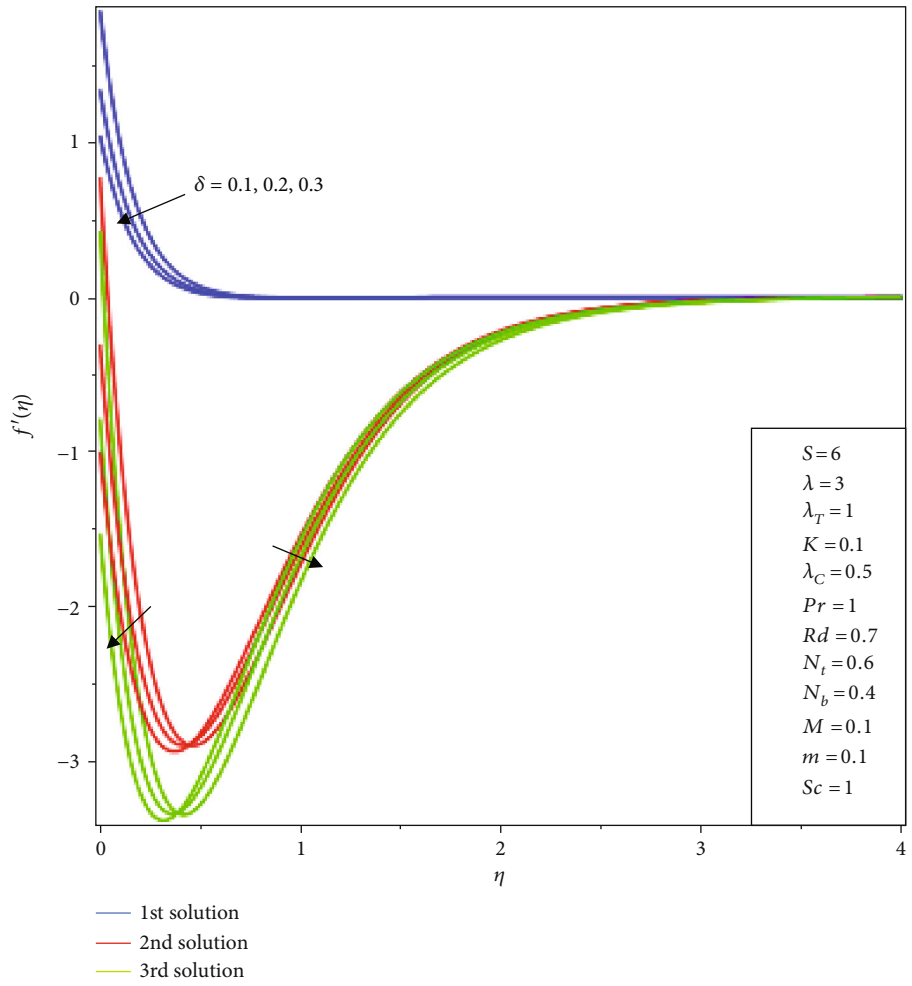

Figure 9: The effects of the δ on the velocity profiles $(f'(\eta))$.

4. Numerical Method

There are presented a short view of the shooting technique (Meade et al. [24]) that is used in Equations (17)–(20) that follow the boundary conditions given in Equation (21). Actually, this method converts the BVPs into the IVPs. So, we have

$$\begin{aligned}
&f' = F_P, f'' = F_{PP}, (1+K)F'_{PP} + FF_{PP} - 2(F_P)^2 + KG_P - 2Mf' + 2\lambda_T\theta + 2\lambda_C\phi = 0,\\
&g' = G_P, \left(1+\frac{K}{2}\right)G'_P + FG_P - 3GF_P - 2KG - KF_{PP} = 0,\\
&\theta' = \theta_P, \phi' = \phi_P, \frac{1}{\mathrm{Pr}}\left(1+\frac{4}{3}\mathrm{R_d}\right)\theta'_\mathrm{P} + \mathrm{F}\theta_\mathrm{P} + \mathrm{N_b}\phi_\mathrm{P}\theta_\mathrm{P} + \mathrm{N_t}(\theta_\mathrm{P})^2 = 0\\
&\phi' = \phi_P, \phi'_P + \mathrm{Sc}F\phi_P + \frac{N_t}{N_b}\theta'_P = 0.
\end{aligned} \tag{53}$$

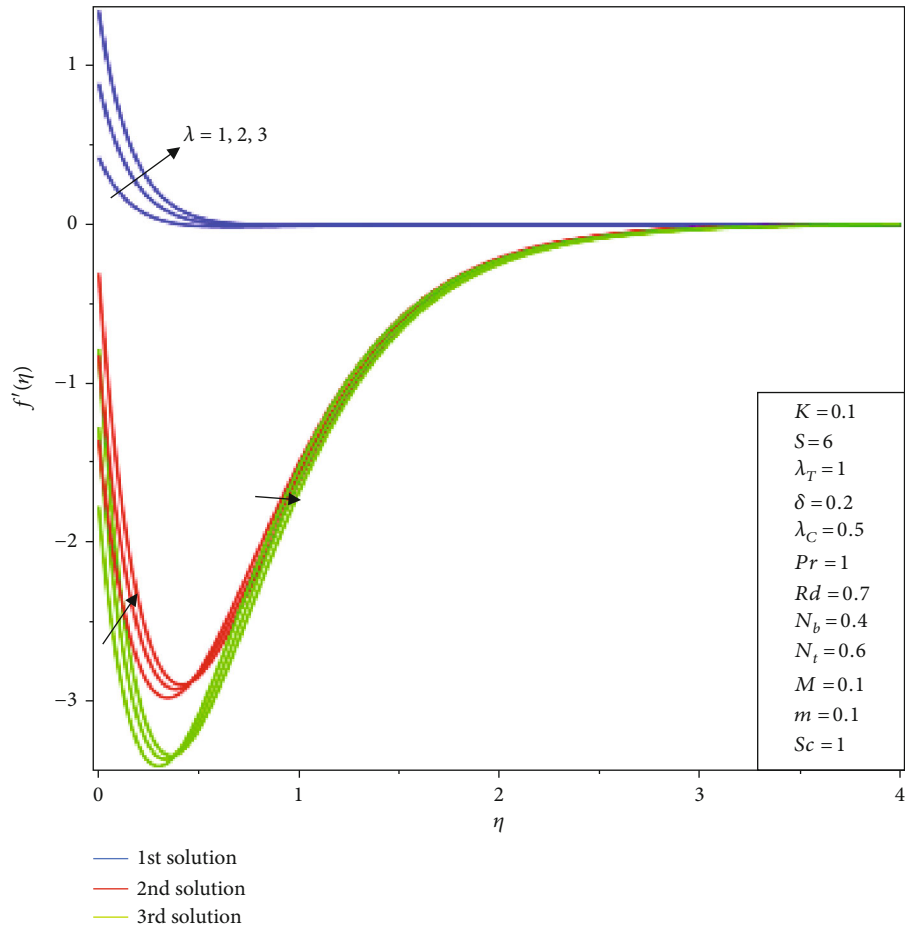

Figure 10: The effects of the λ on the velocity profiles $(f'(\eta))$.

The boundary conditions are

$$\begin{aligned} &F(0) = S\,; F_P(0) = \lambda + \delta\mathfrak{h}_1, F_{PP}(0) = \mathfrak{h}_1, \\ &G(0) = -m\mathfrak{h}_1, G_P(0) = \mathfrak{h}_2, \\ &\theta_P = 1, \theta_P(0) = \mathfrak{h}_3, \\ &\phi(0) = 1\,; \phi_P(0) = \mathfrak{h}_4, \end{aligned} \tag{54}$$

where $\mathfrak{h}_1$, $\mathfrak{h}_2$, $\mathfrak{h}_3$, and $\mathfrak{h}_4$ are the unknown applied initial conditions. Therefore, shooting values of $\mathfrak{h}_1$, $\mathfrak{h}_2$, $\mathfrak{h}_3$, and $\mathfrak{h}_4$ are carefully taken which satisfy the specified boundary conditions of the problem properly. Furthermore, it is noticed that computations of this problem are done by the help of Maple software where shootlib function is added.

5. Result and Discussion

Equations (17)–(20) that subject to the boundary conditions given in Equations (21) are solved numerically by a shooting method in Maple software for the distinct values of used physical parameters. Triple solutions are obtained for different initial guesses at various ranges of specified parameters. Furthermore, for authentication of results, our obtained results have been compared with previously obtained results by the Bidin and Nazar [20], where the comparison indicates a good agreement with our obtained results which are shown in Table 1.

The numerical computations demonstrate the effects of different used physical parameters on skin friction coefficient $(f''(0))$,couple stress coefficient $(g'(0))$, local Nusselt number $(-\theta'(0))$, and Sherwood number $(-\phi'(0))$ as well as on the velocity, microrotation, temperature, and concentration profiles of the micropolar nanofluid which are graphically presented in Figures 2–22. Stability analysis is performed due to occurrence of triple solutions. Therefore, stability analysis is performed by bvp4c in MATLAB programming. The achieved eigenvalues are presented in Table 2, while result of the stability shows that the first solution is the stable and the physically feasible which possesses smallest positive eigenvalues, while negative eigenvalues are found for two other solutions which are declared as unstable and not physically feasible. Therefore, in this article, the result of only first solutions which is physically feasible solutions are presented.

The influence of the material parameter (K) on the skin friction coefficient, couple stress coefficient, Nusselt number, and Sherwood number with variation of stretching/

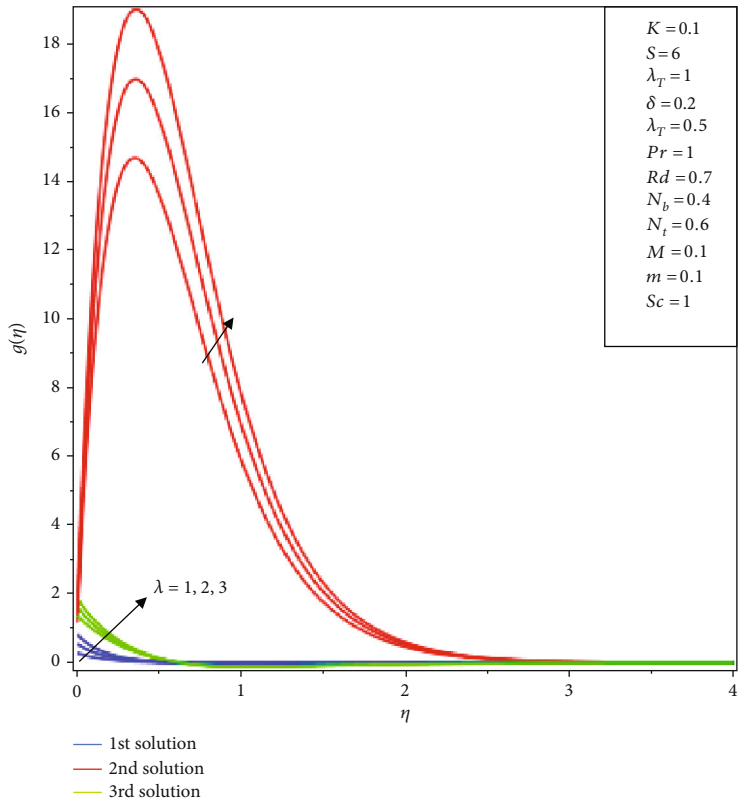

Figure 11: The effects of the λ on the microrotation profiles $(g(\eta))$.

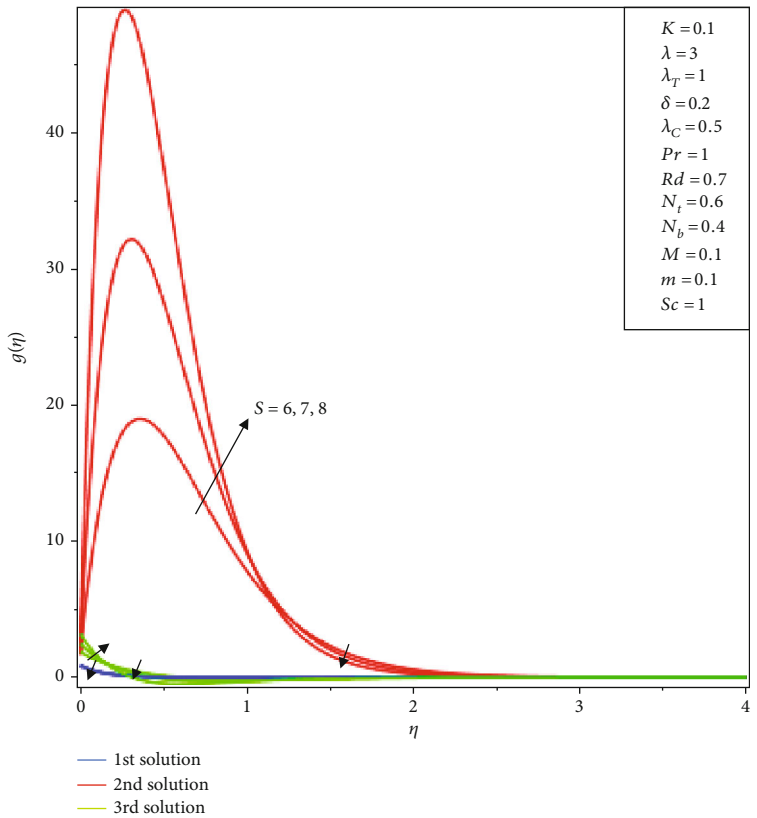

Figure 12: The effects of the S on the microrotation profiles$(g(\eta))$.

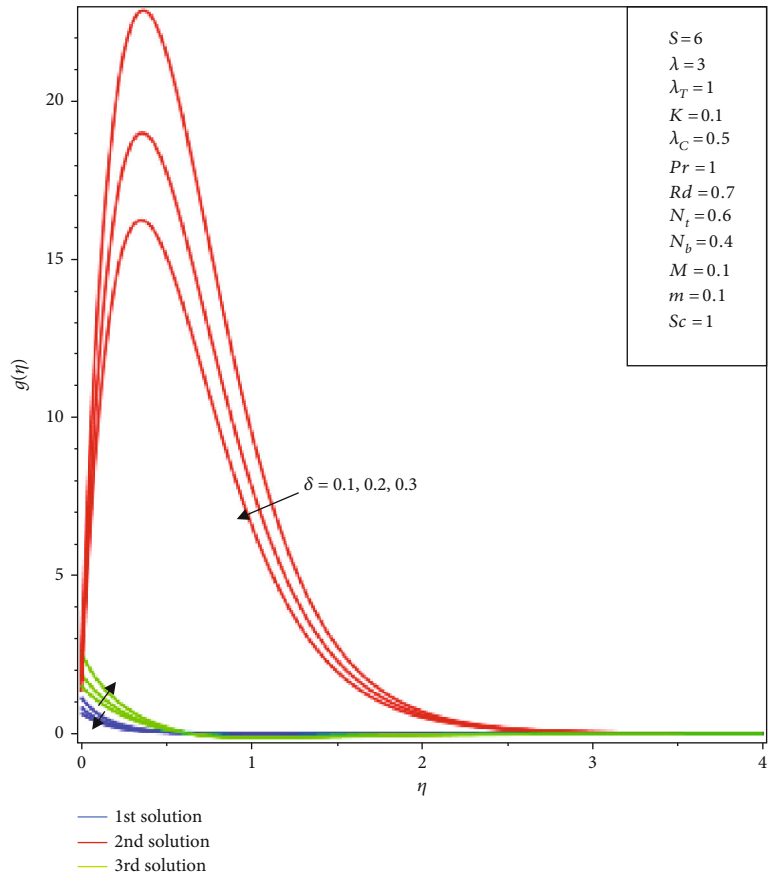

Figure 13: The effects of the δ on the microrotation profiles$(g(\eta))$.

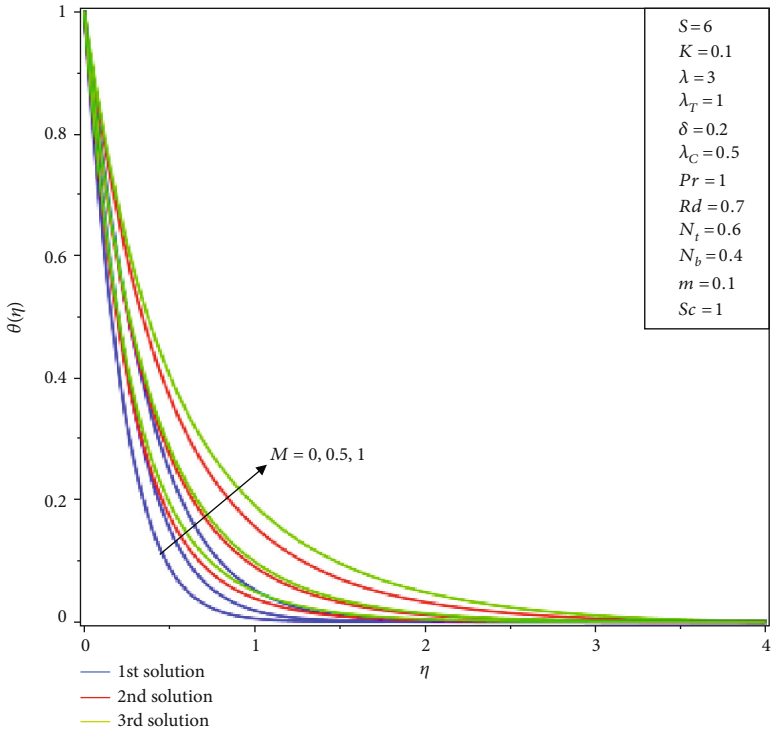

Figure 14: The effects of the M on the temperature profiles $(\theta(\eta))$.

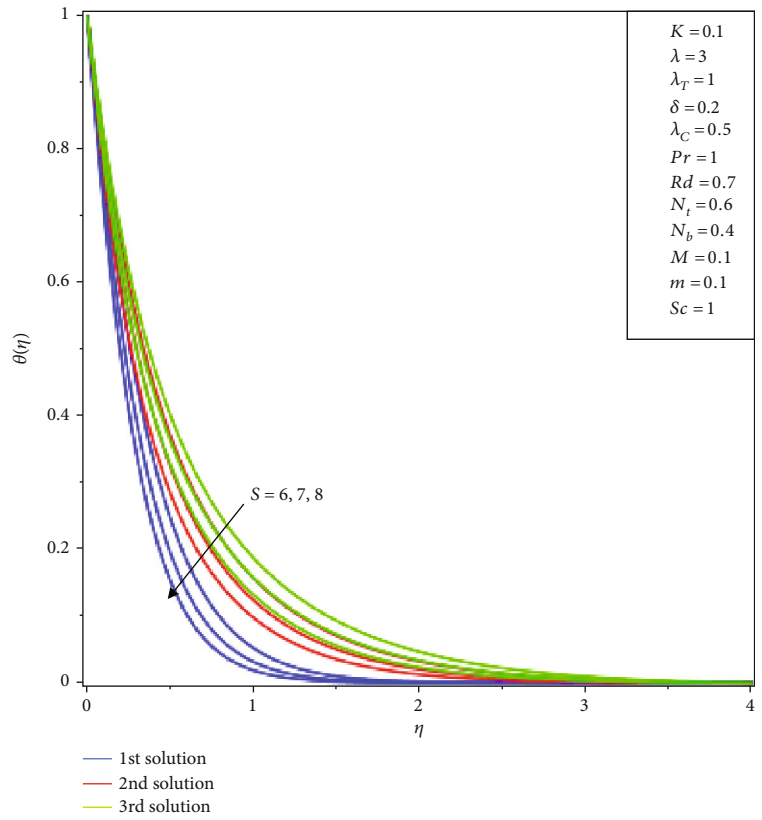

Figure 15: The effects of the S on the temperature profiles ($\theta(\eta)$).

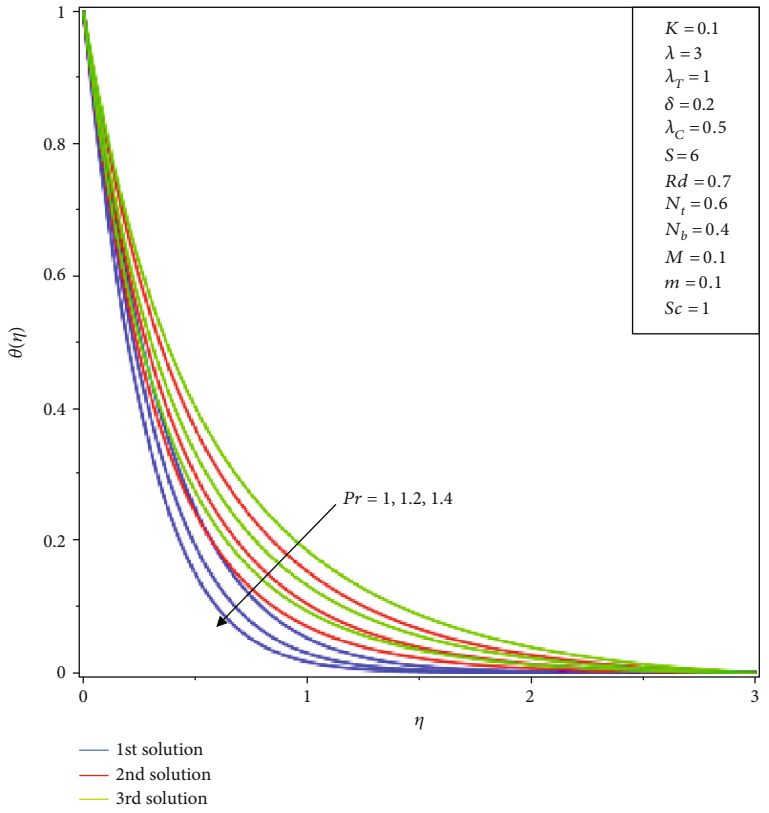

Figure 16: The effects of the Pr on the temperature profiles($\theta(\eta)$).

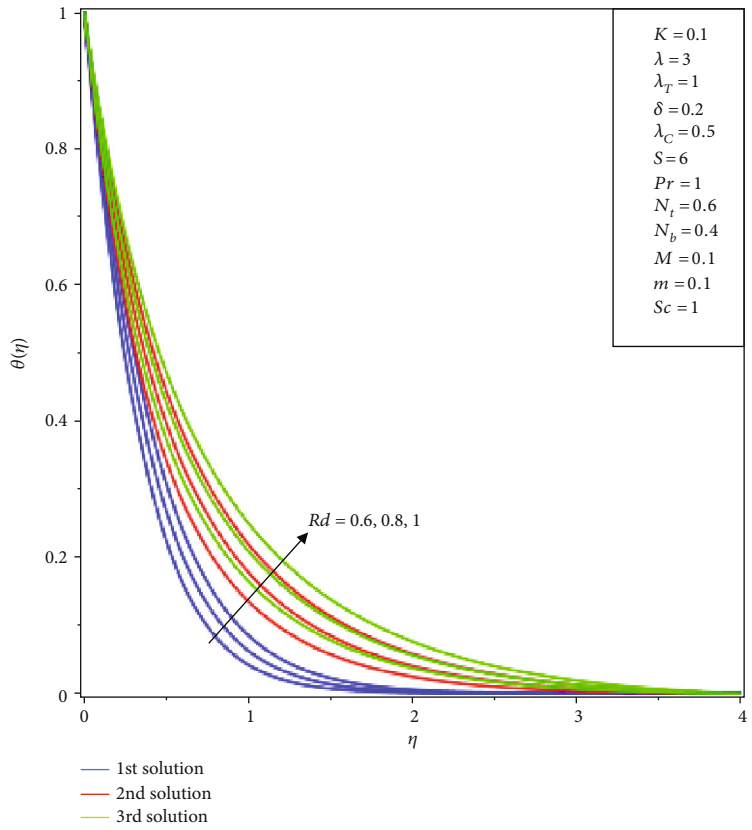

Figure 17: The effects of the R_d on the temperature profiles$(\theta(\eta))$.

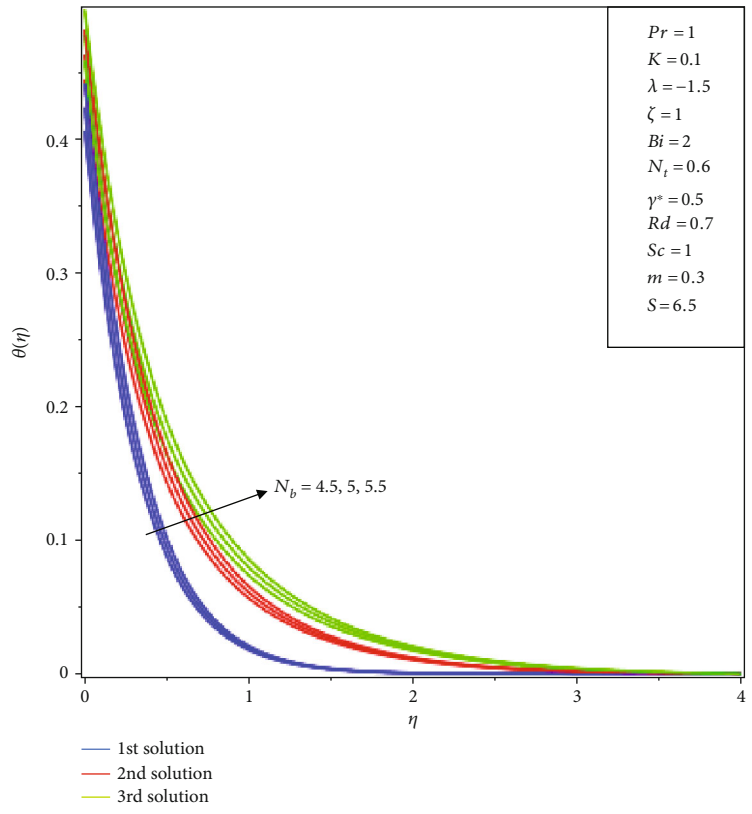

Figure 18: The effects of the N_b on the temperature profiles$(\theta(\eta))$.

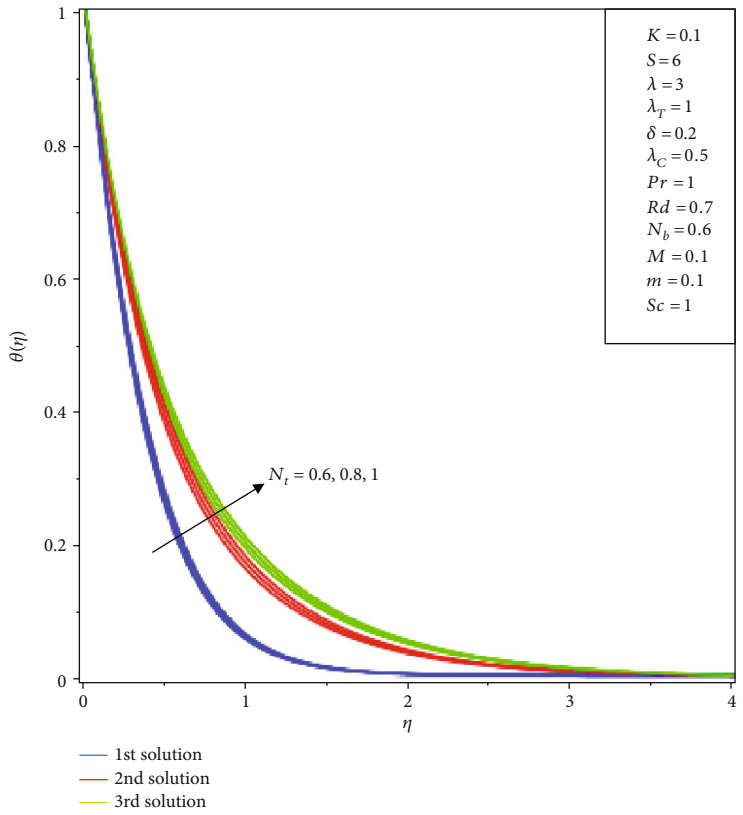

Figure 19: The effects of the N_t on the temperature profiles$(\theta(\eta))$.

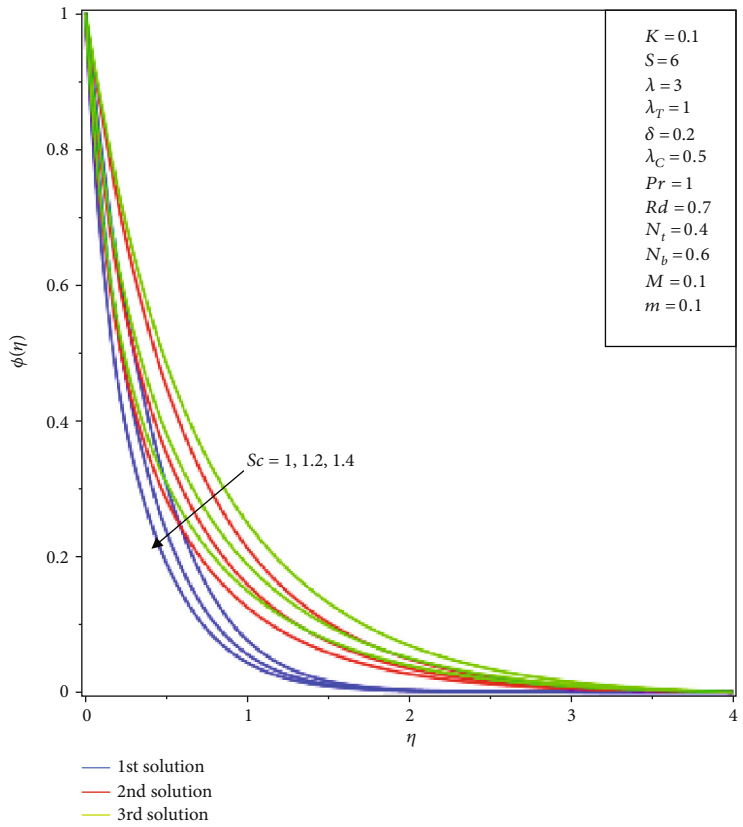

Figure 20: The effects of the S on the concentration profiles$(\phi(\eta))$.

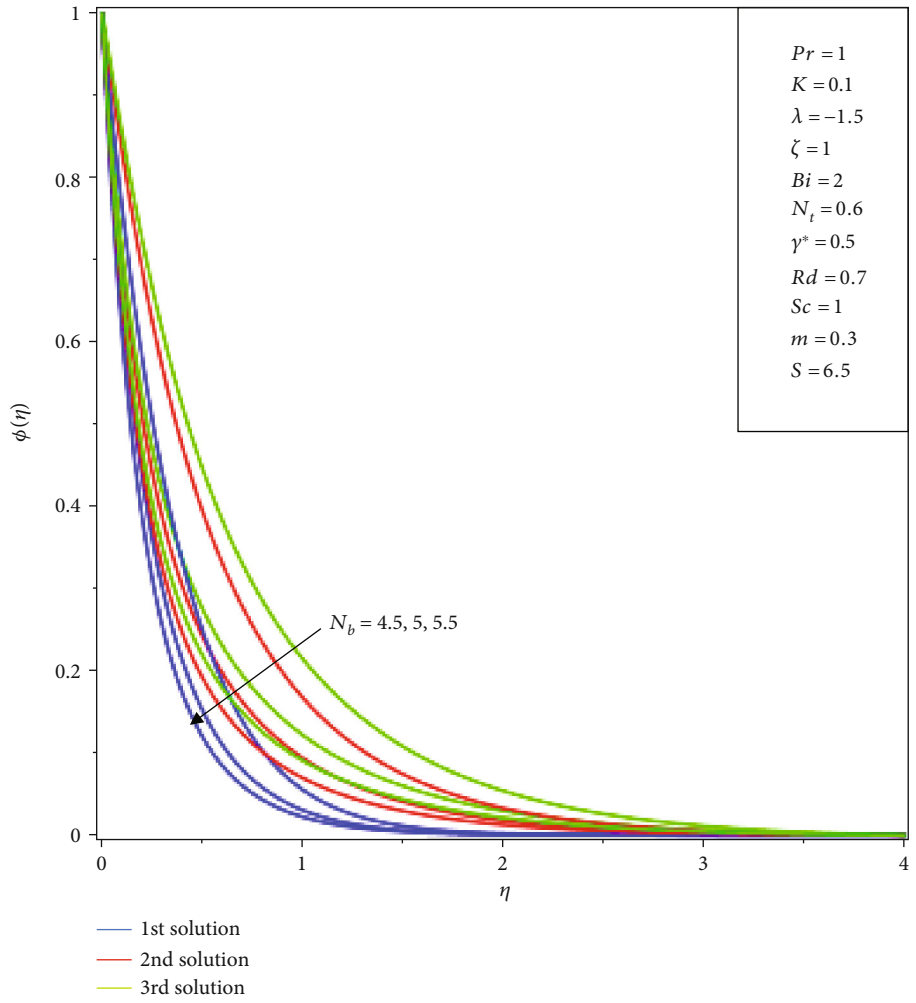

Figure 21: The effects of the N_b on the concentration profiles($\phi(\eta)$).

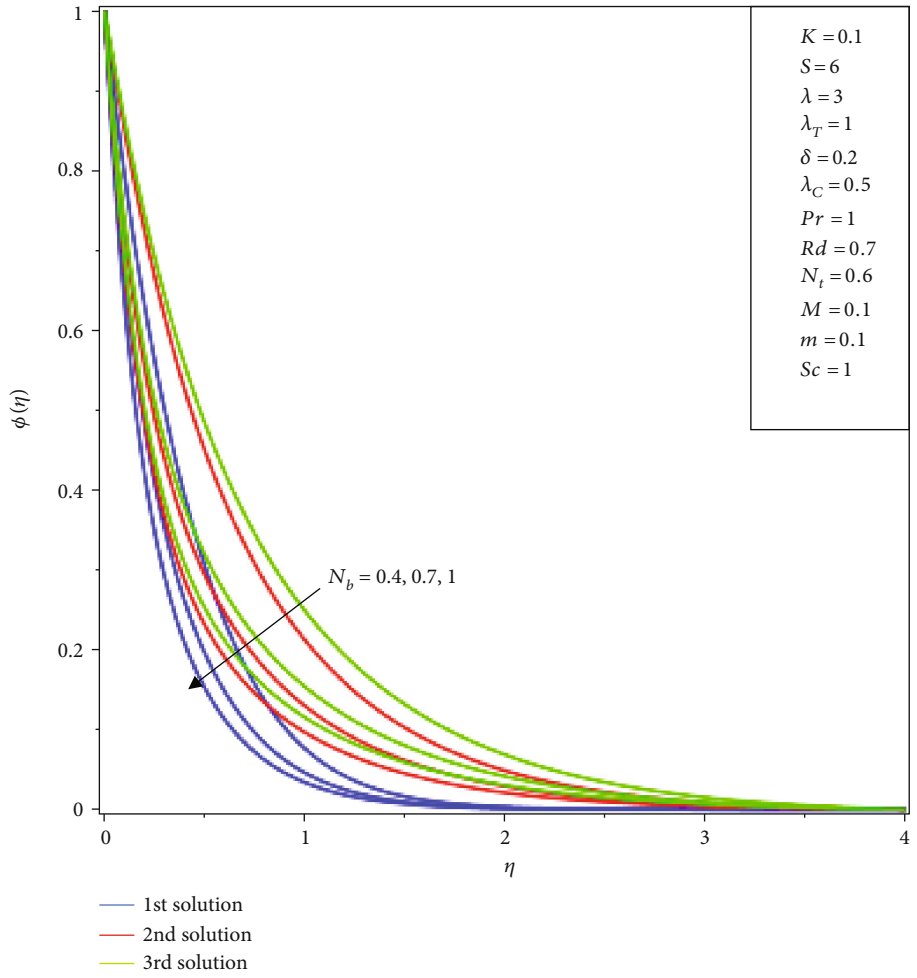

Figure 22: The effects of the N_t on the concentration profiles$(\phi(\eta))$.

Table 2: The smallest obtained eigenvalues (γ_1) at several values of the M and K, where the values of other parameters are fixed as $S = 6$, $\mathrm{Pr} = \mathrm{Sc} = \lambda_T = \lambda = 1$, $\lambda_C = 0.5$, $N_b = 0.4$, $N_t = 0.6$, $R_d = 0.7$, $m = 0.1$, and $\delta = 0.2$.

M	K	γ_1 First solution	Second solution	Third solution
0.1	0.1	1.54340	-1.98503	-2.7911
0.2	0.1	0.09248	-0.43835	-0.96750
0.3	0.1	2.10262	-0.71688	-1.59809
0.1	0.1	0.05824	-0.40107	-2.10521
0.1	0.15	0.63291	-0.20561	-1.90368
0.1	0.2	0.80136	-0.57696	-0.93832

shrinking parameter (λ) are shown in Figures 2–5, where triple solutions are found for $\lambda > \lambda_c$ and unique solution for $<\lambda_c$, while second and third solutions are merged into one another at the point λ_c and only one (first) solution remained continuous for variation of the λ. Furthermore, Figure 2 and Table 3 show that an increase in K with variation in λ increase the skin friction coefficient for the $\lambda > 0$ and decrease for $\lambda < 0$ in the first (stable) solution. Table 3 and Figure 3 indicate that an increase in K along the variation in λ, the couple stress rises for the $\lambda > 0$ and reduces for the $\lambda < 0$. Furthermore, Table 3 defines the numerical results related to the Figures 2 and 3.

Figures 4 and 5 along Table 4 indicate that an increment in the values of K with variation of λ, the Nusselt number, and the Sherwood number increase for $\lambda > 0$ and reduce for $\lambda < 0$ in the first solution throughout the flow of the micropolar nanofluid.

While the effect of magnetic parameter (M) on velocity profile $(f'(\eta))$ is shown in Figure 6, it can be seen that velocity decreases with increase in the parameter M. That occurs due to rising Lorentz forces transverse magnetic field that becomes a reason to decelerate the velocity of the fluid. Figure 7 indicates the influence of thermal convective parameter (λ_T) on velocity profile $(f'(\eta))$. It is seen that the velocity of micropolar nanofluid declines as λ_T is increased. Figure 8 shows the influence of the suction parameter (S) on velocity profile $(f'(\eta))$. It is examined that the increasing rate of the suction decreases the velocity and momentum boundary layer thickness in flow of the micropolar nanofluid. It is because of the flow approaches nearer

Table 3: Computation of skin friction and couple stress coefficient for several values of λ and K.

K	λ	$f''(0)$ 1st solution	$f''(0)$ 2nd solution	$f''(0)$ 3rd solution	$g'(0)$ 1st solution	$g'(0)$ 2nd solution	$g'(0)$ 3rd solution
	-2	5.463761	-3.74033	-8.4974	8.856247	172.091	-15.615
0.1	0	0.247399	-8.04981	-13.135	0.433814	197.318	-20.9
	2	-5.1687	-12.8786	-17.877	-9.33088	211.336	-26.979
	-2	5.2882	-3.85674	-7.038	8.100267	56.6338	-8.4566
0.2	0	0.239959	-7.82914	-11.616	0.408043	69.3817	-14.791
	2	-5.02881	-12.4521	-16.276	-8.66079	73.5664	-21.041
	-2	5.12193			7.421568		
0.3	0	0.232959	-7.85944	-10.129	0.384772	26.4923	-8.2297
	2	-4.89749	-12.2182	-14.789	-8.05949	28.5981	-15.258

Table 4: Computation of local Nusselt number and the Sherwood number for several values of λ and K.

K	λ	$-\theta'(0)$ 1st solution	$-\theta'(0)$ 2nd solution	$-\theta'(0)$ 3rd solution	$-\phi'(0)$ 1st solution	$-\phi'(0)$ 2nd solution	$-\phi'(0)$ 3rd solution
	-2	2.40089	1.95999	1.77551	2.2951	1.53985	1.30019
0.1	0	2.44603	2.03153	1.81838	2.35043	1.61516	1.31665
	2	2.4868	2.09011	1.86953	2.40012	1.67863	1.35093
	-2	2.39719	1.95267	1.82215	2.28999	1.52279	1.34751
0.2	0	2.44599	2.03695	1.86928	2.35043	1.6152	1.37067
	2	2.48968	2.10295	1.92575	2.4042	1.6897	1.41474
	-2	2.39351			2.28482		
0.3	0	2.44593	2.03121	1.92588	2.35042	1.5986	1.43926
	2	2.51407	2.10777	1.98366	2.43491	1.68881	1.48869

to solid surface, so the suction takes place due to porosity of the medium which becomes a reason to decrease the velocity and its boundary layer thickness. Figure 9 illustrates the influence of the velocity slip parameter (δ) on the velocity profile $(f'(\eta))$. It is observed that by rising value of the parameter δ, the velocity profile along the velocity boundary thickness decrease throughout the flow. Actually, the increasing value of δ develops a resistance forces at the surface that becomes the reason to decline the velocity profile, while the effect of parameter λ is found opposite to the influence of the parameter δ on velocity profile of micropolar nanofluid that is shown in Figure 10. Likewise, influence of parameter λ on angular velocity profile $(g(\eta))$ is shown in Figure 11. The figure shows that any increment in λ rises the velocity of the bulk particles that possesses microrotations during the flow. Figure 12 indicates the impact of the parameter S on angular velocity profile $(g(\eta))$. It is seen that an increment in S decelerate the angular velocity related to bulk particles. Figure 13 specifies the effect of the parameter δ on the angular velocity profile $(g(\eta))$. The result of this figure shows that the angular velocity of bulk particles reduces during the flow. The influence of various physical parameters on temperature profiles $(\theta(\eta))$ of micropolar nanofluid are shown by Figures 14–19. Figure 14 indicates that any increment in the parameter M rises the temperature of the micropolar nanofluid during flow. Against it, Figure 15 shows that the increasing rate of suction decreasing the thermal boundary thickness along the temperature profile $(\theta(\eta))$ of the micropolar nanofluid. Actually, this occurs due to rise in suction rate which raises the resistance force between the fluid layers and solid surface. Such sorts of results are observed in Figure 16, when the value of the Prandtl number (Pr) is increased. Actually, higher values of the Prandtl number decreases thermal diffusion of fluid particles which result in the decrease temperature of the fluid. Therefore, increasing the value of the Pr decreases the temperature of the all types of the fluids during the flow. An increase in thermal radiative parameter (R_d) raises temperature and boundary layer thickness during the flow of the micropolar nanofluid that is shown in Figure 17. Actually, the existence of the thermal radiation leads to enhancing the thermal boundary layer thicknesses. Practically, enlarging radiations yields a major enhancement in temperature of fluid. Figures 18 and 19 show the influence of rising the Brownian motion parameter (N_b) and thermophoresis parameter (N_t) on the temperature profiles $(\theta(\eta))$,respectively. The results show that any increment in the mentioned parameters increases the temperature of the particular nanofluid and its boundary layer thicknesses. This takes place because of N_b and N_t increases the temperature gradient at the solid adjacent surface.

Figures 20–22 show the influence of the Brownian motion parameter (N_b), Schmitt number, and thermophoresis parameter (N_t) on nanoparticle concentration profiles $(\phi(\eta))$. Figure 20 shows that an increase in N_b deceases the concentration of the nanoparticles in the micropolar nanofluid throughout the flow. Figure 21 shows the influence of the Schmitt number (Sc) on the concentration profile $(\phi(\eta))$. This figure shows that the concentration of the nanoparticles decreases with increase in the Sc. It is due to increasing the value of Sc which decreases the mass diffusion; the larger diffusion becomes a reason to decrease in the concentration field. Moreover, it also decreases the thickness of the concentration boundary layers, while influence of the N_t looks opposite to the influence of Sc on the concentration profile, where increasing rate of the N_t raises concentration of nanoparticles throughout the flow of micropolar nanofluid.

6. Conclusions

The effects of the various types of physical flow parameters on MHD mixed convection boundary layer flow, heat, and mass transfer of the micropolar nanofluid on exponentially vertical stretching/shrinking surface are studied here. The similarity solutions are achieved by applying similarity transformation from partial differential equations into the ordinary differential equation. The shooting method is implemented to obtain the numerical solution of the equations with variation of the used physical parameters. At various ranges of used parameters, triple solutions are obtained, so the stability is performed by help of the MATLAB through bvp4c. Effects of various used physical parameters such as the magnetic parameter, thermophoresis parameter, microrotation parameter, suction parameter, radiation parameter, Prandtl number, Brownian motion parameter, thermal slip parameter, and Schmidt number are examined, discussed, and also presented graphically. The main results of this study are described below:

(1) Skin friction coefficient, couple stress, Nusselt, and Sherwood numbers are increasing for $\lambda > 0$ and decreasing for $\lambda < 0$ with increase in material parameter (K)

(2) Triple solutions are found at the different ranges of the flow parameters, and from stability analysis, it is found that only first solution is stable as well as physically feasible

(3) The buoyancy parameter and high suction are the leading causes for existence of triple solutions in this problem

(4) The velocity field of the micropolar nanofluid decelerates with increase in the suction parameter (S), magnetic parameter (M), and velocity slip parameter (δ), while increases for increase in thermal convection parameter (λ_T) and stretching parameter (λ)

(5) An increase in parameters M, R_d, N_t, and N_b raises the temperature profiles of the micropolar nanofluid, while it decrease with increase in Pr and S

(6) Any increment in N_t rises the concentration boundary layer thickness and its profile, while an increase in Sc and N_b decreases the concentration boundary layer thickness and its profiles

Nomenclature

x, y: Cartesian coordinates (m)
u, v: Velocity components ($\mathrm{m \cdot s^{-1}}$)
U_w: Shrinking and stretching velocity
K: Material parameter
N: Microrotation
g^*: Gravitational force
T: Temperature (K)
T_∞: Ambient temperature
T_w: Variable temperature at sheet (K)
θ: Dimensionless temperature (K)
C: Concentration ($\mathrm{kg \cdot m^{-3}}$)
C_∞: Ambient concentration ($\mathrm{kg \cdot m^{-3}}$)
C_w: Variable concentration at sheet
β_T: Thermal expansion coefficients
β_C: Concentration expansion coefficients
ϑ: Kinematic viscosity ($\mathrm{m^2 \cdot s^{-1}}$)
K_1: Vortex viscosity ($\mathrm{m^2 \cdot s^{-1}}$)
γ^*: Spin gradient viscosity ($\mathrm{m^2 \cdot s^{-1}}$)
j: Microinertia per unit mass ($\mathrm{kg \cdot m^{-3}}$)
σ^*: Stefan-Boltzmann constant
α: Thermal diffusivity ($\mathrm{m^2/s}$)
ψ: Stream function
η: Transformed variable
q_r: Radiative heat flux ($\mathrm{w/m^2}$)
$B(x)$: Magnetic field ($\mathrm{kg\, s^{-2} A^{-1}}$)
R_d: Thermal radiation
M: Magnetic parameter
Pr: Prandtl number
D_B: Brownian diffusion ($\mathrm{kg \cdot m^{-1} \cdot s^{-1}}$)
D_T: Thermophoretic diffusion ($\mathrm{kg \cdot m^{-1} \cdot s^{-1} \cdot K^{-1}}$)
v_w: Suction/injection velocity ($\mathrm{m \cdot s^{-1}}$)
σ: Electrical conductivity
N_t: Thermophoresis parameter
N_b: Brownian motion parameter
S: Suction/injection parameter
λ: Shrinking/stretching parameter
Sc: Schmidt number
k: Thermal conductivity
m: Constant
C_f: Skin friction coefficient
Nu_x: Local Nusselt number
k^*: Mean absorption coefficient
S_h: Local Sherwood number
Re_x: Local Reynolds number
γ: Unknown eigenvalue
γ_1: Smallest eigenvalue
μ: Dynamic viscosity
τ: Stability transformed variable.

Data Availability

No data was needed to perform this research.

Conflicts of Interest

The authors declare that they have no conflict of interest.

References

[1] A. C. Eringen, "Simple microfluids," *International Journal of Engineering Science*, vol. 2, no. 2, pp. 205–217, 1964.

[2] M. I. Anwar, S. Shafie, T. Hayat, S. A. Shehzad, and M. Z. Salleh, "Numerical study for MHD stagnation-point flow of a micropolar nanofluid towards a stretching sheet," *Journal of the Brazilian Society of Mechanical Sciences and Engineering*, vol. 39, no. 1, pp. 89–100, 2017.

[3] A. R. M. Kasim, N. F. Mohammad, and S. Shafie, "Unsteady MHD mixed convection flow of a micropolar fluid along an inclined stretching plate," *Heat Transfer - Asian Research*, vol. 42, no. 2, pp. 89–99, 2013.

[4] K. Das, "Slip effects on heat and mass transfer in MHD micropolar fluid flow over an inclined plate with thermal radiation and chemical reaction," *International Journal for Numerical Methods in Fluids*, vol. 70, no. 1, pp. 96–113, 2012.

[5] D. Srinivasacharya and K. H. Bindu, "Entropy generation in a micropolar fluid flow through an inclined channel," *Alexandria Engineering Journal*, vol. 55, no. 2, pp. 973–982, 2016.

[6] M. M. Rahman, A. Aziz, and M. A. Al-Lawatia, "Heat transfer in micropolar fluid along an inclined permeable plate with variable fluid properties," *International Journal of Thermal Sciences*, vol. 49, no. 6, pp. 993–1002, 2010.

[7] S. Dero, A. M. Rohni, and A. Saaban, "MHD micropolar nanofluid flow over an exponentially stretching/shrinking surface: triple solutions," *Journal of Advanced Research in Fluid Mechanics and Thermal Sciences*, vol. 56, no. 2, pp. 165–174, 2019.

[8] D. Srinivasacharya, C. RamReddy, and P. Naveen, "Double dispersion effect on nonlinear convective flow over an inclined plate in a micropolar fluid saturated non-Darcy porous medium," *Engineering Science and Technology, an International Journal*, vol. 21, no. 5, pp. 984–995, 2018.

[9] J. Prakash, D. Tripathi, A. K. Tiwari, S. M. Sait, and R. Ellahi, "Peristaltic pumping of nanofluids through a tapered channel in a porous environment: applications in blood flow," *Symmetry*, vol. 11, no. 7, p. 868, 2019.

[10] M. R. Ilias, N. A. Rawi, and S. Shafie, "MHD free convection flow and heat transfer of ferrofluids over a vertical flat plate with aligned and transverse magnetic field," *Indian Journal of Science and Technology*, vol. 9, no. 7, 2016.

[11] S. U. Choi, "Enhancing thermal conductivity of fluids with nanoparticles and applications of non-Newtonian flows," *ASME Journal of Heat Transfer*, vol. 66, pp. 99–105, 1995.

[12] P. Krajnik, F. Pusavec, and A. Rashid, "Nanofluids: properties, applications and sustainability aspects in materials processing technologies," in *Advances in Sustainable Manufacturing*, pp. 107–113, Springer, Berlin, Heidelberg, 2011.

[13] G. Lukaszewicz, *Micropolar Fluids: Theory and Applications*, Springer Science & Business Media, 1999.

[14] J. Buongiorno, "Convective transport in nanofluids," *Journal of Heat Transfer*, vol. 128, no. 3, pp. 240–250, 2006.

[15] S. Dero, A. M. Rohni, A. Saaban et al., "Dual solutions and stability analysis of micropolar nanofluid flow with slip effect on stretching/shrinking surfaces," *Energies*, vol. 12, no. 23, p. 4529, 2019.

[16] L. Ali Lund, D. L. C. Ching, Z. Omar, I. Khan, and K. S. Nisar, "Triple local similarity solutions of Darcy-Forchheimer magnetohydrodynamic (MHD) flow of micropolar nanofluid over an exponential shrinking surface: stability analysis," *Coatings*, vol. 9, no. 8, p. 527, 2019.

[17] R. Nazar, M. Jaradat, N. Arifin, and I. Pop, "Stagnation-point flow past a shrinking sheet in a nanofluid," *Open Physics*, vol. 9, no. 5, pp. 1195–1202, 2011.

[18] A. V. Kuznetsov and D. A. Nield, "Natural convective boundary-layer flow of a nanofluid past a vertical plate," *International Journal of Thermal Sciences*, vol. 49, no. 2, pp. 243–247, 2010.

[19] A. J. Chamkha and A. M. Aly, "MHD free convection flow of a nanofluid past a vertical plate in the presence of heat generation or absorption effects," *Chemical Engineering Communications*, vol. 198, no. 3, pp. 425–441, 2010.

[20] B. Bidin and R. Nazar, "Numerical solution of the boundary layer flow over an exponentially stretching sheet with thermal radiation," *European Journal of Scientific Research*, vol. 33, no. 4, pp. 710–717, 2009.

[21] A. Ishak, R. Nazar, and I. Pop, "Heat transfer over a stretching surface with variable heat flux in micropolar fluids," *Physics Letters A*, vol. 372, no. 5, pp. 559–561, 2008.

[22] A. V. Roşca and I. Pop, "Flow and heat transfer of Powell-Eyring fluid over a shrinking surface in a parallel free stream," *International Journal of Heat and Mass Transfer*, vol. 71, pp. 321–327, 2014.

[23] S. D. Harris, D. B. Ingham, and I. Pop, "Mixed convection boundary-layer flow near the stagnation point on a vertical surface in a porous medium: Brinkman model with slip," *Transport in Porous Media*, vol. 77, no. 2, pp. 267–285, 2009.

[24] D. B. Meade, B. S. Haran, and R. E. White, "The shooting technique for the solution of two-point boundary value problems," *Maple Technical Newsletter*, vol. 3, no. 1, pp. 1–8, 1996.